Electronic Supplementary Material (ESI) for Journal of Materials Chemistry C.
This journal is © The Royal Society of Chemistry 2020

ARTICLE

Supplementary Information

Role of Ln type in the physical mechanisms of defect mediated luminescence of Li, Ln - SnO_2 nanoparticles

Bogdan Cojocaru[1], Claudiu Colbea[2, 3], Daniel Avram[2], Cosmin Istrate[4], Laura Abramiuc[4] and Carmen Tiseanu[, 2]*

[1] Department of Chemistry, University of Bucharest, B-dul Regina Elisabeta, nr. 4-12, 030018 Bucharest, Romania

[2] National Institute for Laser, Plasma and Radiation Physics, RO 76900 Bucharest-Magurele, Romania

[3] Scientific Center for Optical and Electron Microscopy, ETH Zürich, Zürich, Switzerland

[4] National Institute of Materials Physics, 405A Atomistilor Street, 077125 Magurele-Ilfov, Romania

[*]email: carmen.tiseanu@inflpr.ro

Please do not adjust margins

EXPERIMENTAL SECTION

Materials. Lanthanide (Ln=Eu, Sm, Tb, Dy, Er), Li doped SnO_2 were prepared by coprecipitation and citrate complexation method with Li added in concentrations varying from 0 to 15%. The starting materials used in the synthesis of Ln,xLi(bulk)-SnO_2 (x=0, 5, 15% ; Ln= Eu, Sm, Tb or Dy) by coprecipitation method were $SnCl_2.2H_2O$, $Eu(NO_3)_3{\cdot}6H_2O$, $Tb(NO_3)_3{\cdot}6H_2O$, $Dy(NO_3)_3{\cdot}xH_2O$, $Sm(NO_3)_3{\cdot}6H_2O$(Merck), $LiNO_3$ (Alfa Aesar) and NH_4OH (Chemical Company). In a typical coprecipitation synthesis, the tin, lithium and lanthanide precursors (atomic ratio of: 99-x%, x%, 1%) were dissolved in 45 mL distilled water. After complete dissolution, the pH value was adjusted to 10 by dropwise addition of ammonia solution under vigorous stirring. The suspensions were left to age overnight at 60^{o}C. Drying process was composed of an ambient temperature step and a medium temperature step (60^{o}C) coupled with vacuum step. The starting materials used in the synthesis of Ln,xLi(bulk)-SnO_2 (x=0, 5, 15% ; Ln= Eu, Sm, Tb or Dy) by citrate complexation method were $SnCl_2.2H_2O$, $Eu(NO_3)_3{\cdot}6H_2O$, $Tb(NO_3)_3{\cdot}6H_2O$, $Dy(NO_3)_3{\cdot}xH_2O$, $Sm(NO_3)_3{\cdot}6H_2O$(Merck), $LiNO_3$ (Alfa Aesar) and Citric acid (Chemical Company). In a typical citrate synthesis, the tin, lithium and lanthanide precursors (atomic ratio of: 99-x%, x%, 1%) were dissolved in 25mL distilled water at 70°C. The proper mixing was established by vigorous stirring for one hour. Citric acid (Sn-CA molar ratio is 1:1.2) was quickly added to the reaction mixture and after one hour the product was dried in a rotary evaporator. The obtained gel was dried in an oven under vacuum at 70 °C for four hours and overnight at 120°C without vacuum. Irrespective of the synthesis approach, the Ln(Li) SnO_2 samples were calcined at 800^{o}C for 4 hours with a heating/cooling rate of 10 ^{o}C/min. Li free, Ln-SnO_2 obtained by the two methods described above were also calcined at 1000 ^{o}C using similar thermal treatment conditions as mentioned above and were further used as reference samples.

Characterization. The crystalline structure was studied by X-Ray Diffraction (XRD) using a Brucker D8 Advance diffractometer (Cu Kα radiation-40Kv, 40mA, Bragg-Bretano geometry, at a scanning speed of

 This journal is © The Royal Society of Chemistry 20xx

Please do not adjust margins

0.1°/min, in the 2θ range 10-90 with a step size of 0.02° and a step time of 2 seconds). Particle size was determined using Scherrer equation [1](1) $L = \frac{K\lambda}{\beta\cos\theta}$ where λ is the wavelength in nanometer, β is the peak width of the diffraction peak profile at half maximum height resulting from small crystallite size in radians, K is the shape factor which was considered 0.9 in our study and θ is the Bragg angle. Cell parameters were determined with MAUD software with its dedicated function based on the following formula: (2) $\frac{1}{d^2} = \frac{h^2+k^2}{a^2} + \frac{l^2}{c^2}$ where d is the interplanar distance, a and c are the cell parameters, h, k and l are the Miller indices. Diffuse Reflectance Infrared Fourier Transform Spectroscopy (DRIFT) spectra were measured on a Brucker Tensor II spectrometer using Harrick Praying Mantis as a diffuse reflectance accessory. Spectra were recorded at 4 cm^{-1} nominal resolution and 100 scans studies. Raman spectra were acquired with 0.7 cm^{-1} resolution in the extended spectral region from 150 up to 4000 cm^{-1}. Raman analysis was carried out with a Horiba Jobin Yvon LabRAM HR UV–visible–NIR Raman microscope spectrometer (~0.4 μm resolution on *X* and *Y* axes and ~0.7 μm resolution on *Z* axe) at 514 nm.

TEM results were obtained using the analytical transmission electron microscopy JEM ARM 200F, at an acceleration voltage of 200 kV. X-ray photoelectron spectroscopy (XPS) measurements were performed in an ESCALAB Xi+ (Thermo SCIENTIFIC Surface Analysis) setup equipped with a multichannel hemispherical electron Analyzer (dual X-ray source) working with Al Kα radiation (hv=1486.2 eV), using C 1s (284.4 eV) as the energy reference. XPS data were recorded by slightly pressing powdered materials that had been outgassed in the pre-chamber of the instrument at room temperature at a pressure of <2 × 10^{-8} Torr to remove chemisorbed water from their surfaces.

Luminescence spectroscopy. The photoluminescence (PL) measurements were carried out using a Fluoromax 4 and a Fluorolog 3 spectrofluorometer (Horiba) operated in fluorescence mode. The digital images were obtained in the *dark room light conditions* by use of Canon EOS 60D under exposure time of

Please do not adjust margins

1 s with 400 ISO. Time-resolved emission spectra and emission decays were recorded using a wavelength-tunable (from 210 to 2300 nm) NT340 Series EKSPLA OPO (Optical Parametric Oscillator) operated at 10 Hz as excitation light source. The tunable wavelength laser has a narrow linewidth < 4 cm^{-1} with a scanning step varying from 0.05 to 0.1 nm. As a detection system, an intensified CCD (iCCD) camera (Andor DH720) coupled to a spectrograph (Shamrock 303i, Andor) was used. Photoluminescence (PL) was detected with a spectral resolution of 0.44 nm and the input slit of the spectrograph was set to 10 µm. For the emission decay measurements in the visible spectral range, a PMT module (PMA-C 192-N-M, PicoQuant GmbH) with appropriate filters and a PCIe TCSPC card TimeHarp 260 NANO (PicoQuant GmbH) as an acquisition system was used. For the very weak luminescence signal, "Photon Counting" mode of the iCCD camera was employed. Photon counting mode carries the key benefit that it is a means to circumvent the Multiplicative Noise. Multiplicative noise is a by-product of the Electron Multiplication process and affects ICCD. This gives the new 'effective shot noise' that has been corrected for multiplicative noise. Photon Counting mode does not measure the exact intensity of a single photon spike but instead registers its presence above a threshold value. It does this for a succession of exposures (more than 1000 exposures for a good signal to noise ratio) and combines the individual 'binary' spectra to create the final emission spectrum. For the emission decay measurements in the near-infrared spectral range, a NIR PMT module (H10330B-75, Hamamatsu) detector coupled to a spectrograph/monochromator (Acton SP2758, Princeton Instruments) and a PCIe TCSPC card TimeHarp 260 NANO (PicoQuant) was employed. The average decay lifetimes were estimated by integrating the area under the normalized emission decays: $\bar{\tau} = \int_0^\infty tI(t)dt / \int_0^\infty I(t)dt$, where $I(t)dt$ is the normalized decay law.

 This journal is © The Royal Society of Chemistry 20xx

Please do not adjust margins

Table S1: Crystallite size, cell parameters, cell volume, strain and bandgap values of Eu(Er), xLi - SnO_2

Sample name	Cryst. size(nm) (±0.5nm)	Cell parameter a/b (±0.05 Å)		Cell volume	Lattice strain		Band gap (eV)
					ε_{110}/ ε_{110}*10^{-3}		
Eu-R	16.6	4.738 /3.186		71.526	2.824	0.929	2.42
Eu, 0Li	11.6	4.740	3.192	71.699	3.446	0.99	2.44
Eu, 5Li	15.5	4.740	3.186	71.594	2.556	0.79	2.65
Eu,10Li	16.3	4.740	3.187	71.609	2.507	0.771	2.68
Eu, 15Li	18	4.739	3.186	71.567	2.237	0.753	2.7
Er, 0Li	14	4.739	3.185	71.525	3.217	0.818	2.41
Er, 5Li	15.9	4.741	3.187	71.634	2.437	0.734	2.55
Er, 10Li	20.1	4.742	3.187	71.693	2.213	0.633	2.63
Er, 15Li	22.6	4.743	3.187	71.689	2.508	0.679	2.65
Er-R	21.6	4.741	3.184	71.565	2.574	0.792	2.40

Footnote: Lattice constants according to PDF 01-079-5607 a=b=4.738 Å, c=3.187 Å; Lattice constants of tetragonal SnO_2 were calculated, using (110) and (101) scattering planes from ~26.5 and 33.8 degrees, using a full pattern fit derived from the reference PDF card** Lattice strain was calculating using the equation $\varepsilon = \frac{\beta}{4tan\theta}$, where θ is the Bragg diffraction angle and β is the FWHM expressed in radians.

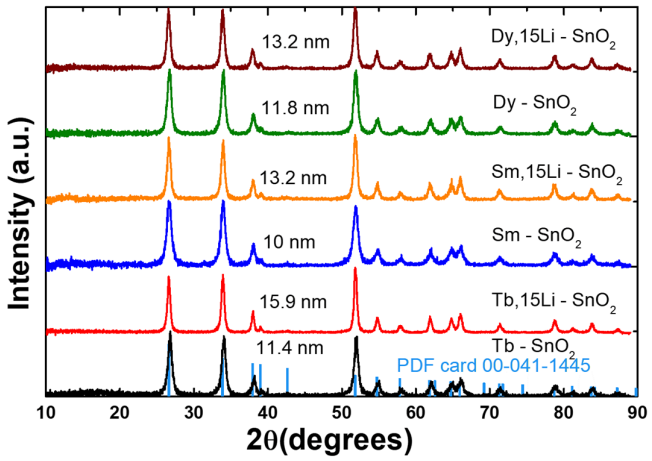

Figure S1. XRD patterns of Li free and Dy/Sm/Tb-15Li-SnO_2. Standard PDF card of SnO_2 is included as reference.

This journal is © The Royal Society of Chemistry 20xx

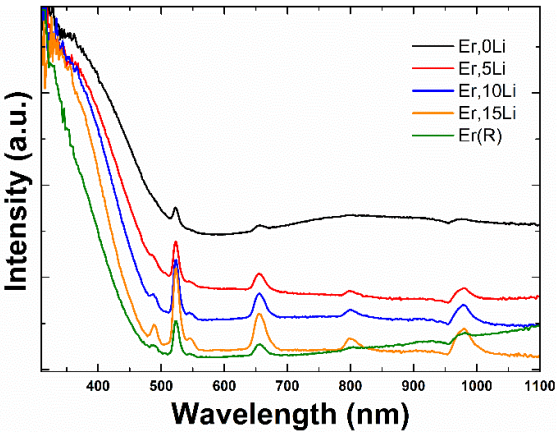

Figure S2. Diffuse reflectance spectra of Er,Li-SnO_2 series and Er-SnO_2 reference (R) sample.

Please do not adjust margins

Note S1

The spectra are 'deconvoluted' (i. e. simulated) by using Voight line shapes (which model the combined effect of core hole and experimental broadenings) combined with integrals of Voigt profiles for taking into account the associated background due to inelastic scattering of photoelectrons on their way out of the sample[2]. Each line from XPS spectrum represents a different chemical state of emitting atoms. If the associated inelastic background is important with respect to the intensity of the main line, that means that in average the emitting atoms are located deeper in the bulk, within the range of a few inelastic mean free paths. If the amplitude of the inelastic background tends to zero, this is a sign that the emitting atoms responsible for the line in question are located near the surface of the sample[3]. Therefore, in some cases the amplitude of the associated inelastic background allows one to trace not only the chemical state, but also the position (surface or bulk) of the atoms in question. This seems to be the case for Eu 3d5/2 spectra (**Figure 2a**), where the main structure is fitted with two lines, one of lower binding energy and important inelastic background and one of higher binding energy and vanishing inelastic background, i. e. due to surface atoms. Other suboxides might also be present in the low binding energy region of Sn 3d spectra (**Figure 3a**), but one cannot fit this low signal region with a large number of components. One may also question why inelastic backgrounds are considerably lower for Sn 3d and O 1s than for Eu 3d5/2 and the answer is connected with the inelastic mean free path of the photoelectrons, which increases exponentially with the kinetic energy of the photoelectrons. Electrons from the Eu 3d5/2 spectra have the lowest average kinetic energy of all the spectra represented here, about 1487 - 1135 = 352 eV, and the corresponding inelastic mean free path is about 8 Å, while for the other core levels, with kinetic energies in the range of 1 keV, the inelastic mean free path is in the range of 20 Å [4].

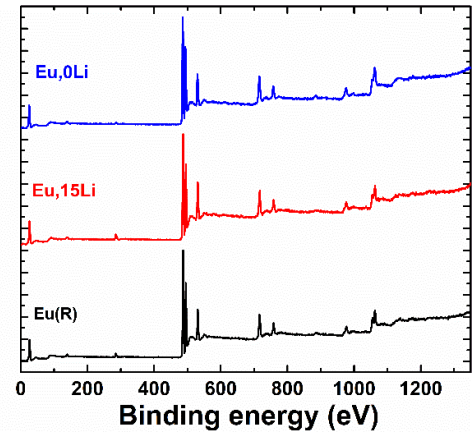

Figure S3. XPS survey spectra of Eu, 0Li - SnO_2, Eu,15Li-SnO_2 and Eu- SnO_2 (R) samples.

This journal is © The Royal Society of Chemistry 20xx

Please do not adjust margins

Please do not adjust margins

Note S2

The comparison of the emission intensity between Ln,xLi and R samples was made using the same geometrical setup in the Xe lamp-based spectrofluorometer and a standard sample holder (14 × 7 mm). The powder samples were compacted in the sample holder to obtain similar powder density (leading to similar light reflection/transmission). The powder in the sample holder was exposed to a limited excitation light spot using a mechanical iris to assure the same sample surface is excited across all samples. For the estimation of enhancement factors, the peak excitation wavelength was set to maximum SnO_2 absorption (obtained from the excitation spectra) using the maximum slit available of 29 nm in excitation and 1 nm in emission. The final values resulted from an average of five measurements.

For center selective laser excited measurements, all the emission spectra were measured using the same setup geometry, sample quantity and holder position and emission slit. To account for the different emission intensity, only the detection reading variables were changed (the delay and gate width, the multichannel plate gain and the number of accumulations).

This journal is © The Royal Society of Chemistry 20xx

Please do not adjust margins

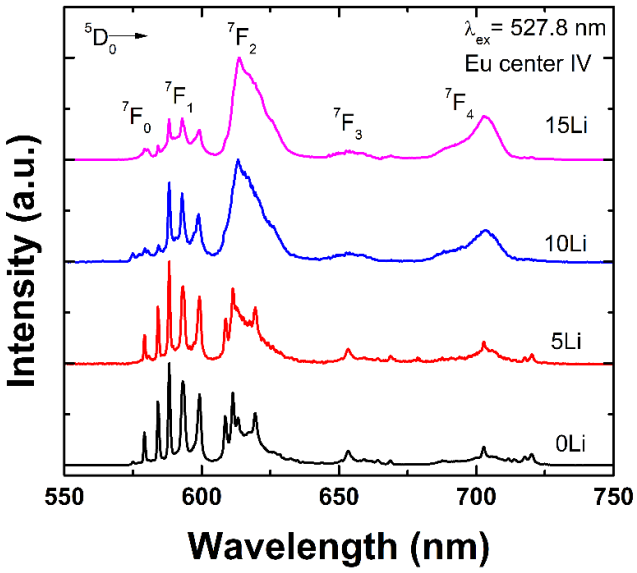

Figure S4. Effects of Li co-doping on the luminescence properties of Eu center **IV** (figure associated with **Figure 3**).

This journal is © The Royal Society of Chemistry 20xx

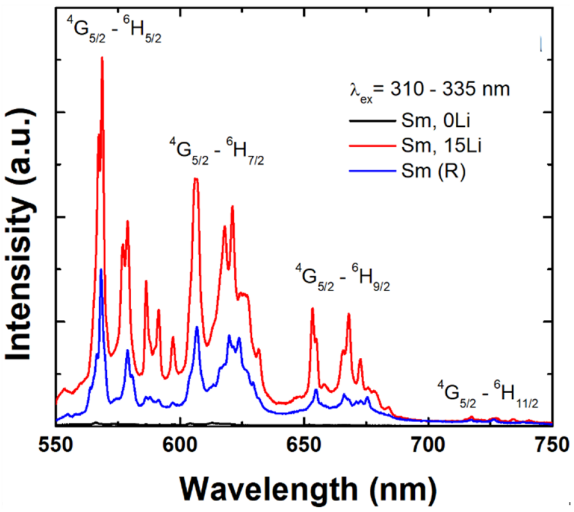

Figure S5. Effects of Li co-doping on the luminescence spectra of Sm-SnO_2 (isolated substitutional center).

The luminescence spectra of substitutional isolated Sm center are dominated by the magnetic dipole (MD) $^4G_{5/2}$ - $^6H_{5/2}$ emission transition (560 - 570 nm) followed by the mixed electric dipole (ED) and MD $^4G_{5/2}$ - $^6H_{7/2}$ emission transition (600 - 640 nm) and the ED $^4G_{5/2}$- $^6H_{9/2}$ emission transition (645 - 700 nm) [5-7]. The luminescence spectra of Sm, 0Li sample too low to be accurately measured. Such low emission generates an additional error when calculating the enhancement factor. The estimated enhancement factors of 40 for Li co-doped sample and 12 for R sample have associated error of ~20 %. By contrast, the enhancement factors for Eu and Er were estimated with an error less than 3%.

References:

1. A. L. Patterson, *Physical Review*, 1939, **56**, 978-982.
2. C. Teodorescu, J. Esteva, R. Karnatak and A. Elafif, *Nuclear Instruments & Methods in Physics Research Section a-Accelerators Spectrometers Detectors and Associated Equipment*, 1994, **345**, 141-147.
3. D. Mardare, D. Luca, C. Teodorescu and D. Macovei, *Surface Science*, 2007, **601**, 4515-4520.
4. S. Hüfner, *Photoelectron spectroscopy: Principles and applications*, Springer, Berlin, 2013.
5. W. T. Carnall, P. R. Fields and K. Rajnak, *The Journal of Chemical Physics*, 1668, **49**, 4424-4442.
6. P. Solarz and W. Ryba-Romanowski, *Physical Review B*, 2005, **72**.
7. C. M. Dodson and R. Zia, *Physical Review B*, 2012, **86**, 125102.